Nuclear Wavepacket Motion between P* and $P^+B_A^-$ Potential Surfaces with Subsequent Electron Transfer to H_A in Bacterial Reaction Centers. 1. Room Temperature†

Andrei G. Yakovlev,‡ Anatoli Ya. Shkuropatov,§ and Vladimir A. Shuvalov*,‡,§

Department of Photobiophysics, Belozersky Institute of Chemical and Physical Biology of Moscow State University, Moscow 119899, Russia, and Institute of Basic Biological Problems, Russian Academy of Sciences, Pushchino, Moscow region 142292, Russia

Received December 3, 2001; Revised Manuscript Received January 19, 2001

ABSTRACT: Formation and coherent propagation of nuclear wavepackets on potential energy surfaces of the excited state of the primary electron donor P* and of the charge transfer states $P^+B_A^-$ and $P^+H_A^-$ were studied in native and pheophytin-modified *Rhodobacter sphaeroides* R-26 reaction centers (RCs) induced by 25 fs excitation (where B_A and H_A are the primary and secondary electron acceptors, respectively). The processes were monitored by measuring coherent oscillations in kinetics of the time evolution of the stimulated emission band of P* at 935 nm, of the absorption band of B_A^- at 1020 nm, and of the bleaching band of H_A at 760 nm. It was found that the nuclear wavepacket motion on the 130−140 cm^{-1} surface of P* is directly induced by light absorption in P. When the wavepacket approaches the intersection between P* and $P^+B_A^-$ surfaces at 120 and 380 fs delays, the formation of intermediate mixed-state emitting light at 935 nm (P*) and absorbing light at 1020 nm ($P^+B_A^-$) takes place. At the latter time, the wavepacket is transferred to the 32 cm^{-1} mode which can belong to the P* hypersurface effectively transferring the wavepacket to the $P^+B_A^-$ surface or can represent a diabatic surface which is formed by the states P* and $P^+B_A^-$. The wavepacket motion on the $P^+B_A^-$ surface or on the $P^+B_A^-$ part of the mixing surface is accompanied by irreversible electron transfer to H_A. This process is monitored by the kinetics of 1020 nm band development and 760 nm band bleaching (delayed with respect to 1020 nm band development) which both have the enhanced 32 cm^{-1} mode in Fourier transform (FT) spectra. The mechanism of wavepacket transfer from the 130−140 cm^{-1} to the 32 cm^{-1} mode is discussed.

Highly efficient primary charge separation in the bacterial hexachromophoric reaction center (RC)[1] protein occurs from the excited singlet state of the primary electron donor (bacteriochlorophyll dimer, P). An electron is transferred from P* to the primary electron acceptor B_A (bacteriochlorophyll monomer located in the photoactive cofactor branch A) within ∼3 ps in *Rb. sphaeroides* RCs at room temperature (*1*, *2*) and ∼1.5 ps at low temperature (*3*) with the formation of the charge-separated state $P^+B_A^-$. Subsequently, an electron is transferred from B_A^- to H_A (bacteriopheophytin in the branch A) to yield state $P^+H_A^-$. This process occurs faster than the initial electron transfer from P* to B_A and takes ∼0.9 ps at room temperature (*2*) [∼300 fs at low temperature (*4*)].

The formation of P* is accompanied by the bleaching of the ground-state absorption bands of P at 600 nm (Q_x transition) and at 870 nm (Q_y transition) and by a development of stimulated emission from P* around 920 nm. The stimulated emission from P* decays within ∼3 ps (*5*) [1.5 ps at low temperature (*3*, *5*)], that corresponds to a time constant of the electron transfer (ET) from P* to B_A. The formation of state $P^+B_A^-$ is characterized by the bleaching of the absorption bands of P at 600 and 870 nm, by the bleaching of B_A bands at 600 nm (Q_x transition) and 800 nm (Q_y transition), and by the formation of the P^+ band at 1250 nm and the B_A^- band at 1020 nm (*2*, *3*). The formation of state $P^+H_A^-$ results in the P bands bleaching and in the bleaching of the H_A absorption bands at 545 nm (Q_x transition) and 760 nm (Q_y transition), in a blue shift of the B_A band at 800 nm, and in the development of the radical anion bands of H_A^- at 660, 910, and 960 nm (*6*). The free energy level of $P^+B_A^-$ was found to be below that of P* by 350−550 cm^{-1} (*7*, *8*). The energy of $P^+H_A^-$ lies below that of P* by ∼2000 cm^{-1} (*9*). Some investigators [see (*10*)] suggest that an electron is directly transferred from P* to H_A without real participation of B_A as an intermediate electron carrier. The observation by several groups (*2*, *3*, *11*, *12*) of femtosecond formation of the B_A^- band at 1020

† This work was supported by the Russian Basic Research Foundation (Grant N 99-04-49120), "Universities of Russia−Basic Researches", INTAS, and NWO (The Netherlands).

* To whom correspondence should be addressed. Fax: (7) (096) 7790532. E-mail: shuvalov@issp.serpukhov.su. Phone: (7) (096) 7733601.

‡ Belozersky Institute of Chemical and Physical Biology of Moscow State University.

§ Russian Academy of Sciences.

[1] Abbreviations: Δ*A*, light-minus-dark absorbance changes; B_A and H_A, the primary and secondary electron acceptors, respectively, located in active branch A; RC, reaction center; ET, electron transfer; FT, Fourier transform; P, primary electron donor; Pheo, pheophytin.

10.1021/bi0101244 CCC: $22.00
Published on Web 02/01/2002

nm within ~3 ps at room temperature (*2, 11, 12*) [~1.5 ps at low temperature (*3*)] strongly supports two-step ET in RCs.

Charge separation in RCs between spectrally separated chromophores allows a study of coupling of nuclear motions and electron transfer. Several methods are available for such a study. The first and detailed description of the vibration structure of the P absorption band was done by the hole burning experiments at 1.7 K in closed RCs (in the presence of H_A^-) (*13*). It has been shown that the zero-phonon line (width less than 1 cm^{-1}) for the P band bleaching near the 0−0 transition is accompanied by two clear vibration modes at ~30 and ~140 cm^{-1} (*13*). The modes at 73, 110, 175, and 205 cm^{-1} were observed as well. Similar modes were found by the resonance Raman at 34, 71, 95, and 128 cm^{-1} (*14*−*16*).

Recently, femtosecond coherence spectroscopy has offered a new tool for the observation of low-frequency nuclear motions induced by light (*17*−*22*). Excitation of P by ultrashort pulses (<30 fs) of broad spectral width leads to the formation of a superposition of many vibrational wave functions that create a wavepacket having time-dependent position on the potential energy surfaces. Such a nuclear motion can be visualized by the femtosecond oscillations in the kinetics of stimulated emission from P* (*19*). Because of a displacement of the potential energy surface of P* with respect to that of P, the stimulated emission from the wavepacket on the P* surface to that on the P surface has a time-dependent spectral position. As a result, the long- and short-wavelength emission components are out-of-phase to each other but have the same oscillation frequencies. FT spectra of the oscillations at low and room temperatures show vibrational modes at 15, 30, 69, 92, 122, 153, 191, and 329 cm^{-1} (*19*) similar to those found in hole burning experiments (*13*) and by Raman spectroscopy (*14*−*16*).

The fundamental aspect of usage of femtosecond spectroscopy is a possibility of a direct study of coupling between nuclear motions and primary ET in the subpicosecond and picosecond time domains. Such a possibility was shown by femtosecond measurements of the kinetics with respect to zero line near 800 nm (B_A absorption band) (*22*) and of the kinetics with spectral analysis near 1020 nm (B_A^- absorption band) in pheophytin-modified RCs from *Rb. sphaeroides* at room temperature (*11, 12*). The attempt (*21*) to observe B_A^- band formation near 1020 nm by one-wavelength kinetic measurements using 100 fs pulses failed probably due to a strong contribution from oscillations of the stimulated emission from P* in this region. In fact, if the absorbance changes at 1020 nm include the stimulated emission of P* and the absorbance increase due to B_A^- formation, the one-wavelength measurements of the kinetics at 1020 nm with respect to the zero line show the development of the two mentioned processes. However, if the absorbance changes for the B_A^- band have a narrower spectral feature than the stimulated emission band [see Figure 1 of (*11*)], the development of the 1020 nm band on the broad background can be measured by spectral analysis at each femtosecond delay. By this approach, the kinetics related only to B_A^- formation were measured (*11, 12*). On the other hand, if 1020 nm band formation and the stimulated emission band of P* are in-phase with approximately equal amplitudes but with opposite direction (absorbance increase and decrease, respectively), the one-wavelength kinetic measurements with respect to the zero line should show nothing. This is probably the case for the measurements in (*21*). Using 110 fs pulses in that work creates another principle problem described by Vos et al. (*19*) and related to the absence of femtosecond oscillations higher than 15 cm^{-1}.

The same arguments are true for the measurements of the H_A band at 760 nm, which is spectrally narrower than the bands related to the formation and decay of P* and $P^+B_A^-$ in this spectral region. Kinetics measured on the basis of the spectral analysis near 760 nm at each delay can show real kinetics of the development of $P^+H_A^-$. Therefore, the whole spectrum measurements in this region during one flash were used to observe the development and disappearance of the 1020 nm band and the disappearance of the 760 nm band in the present work.

It was found that in native and pheophytin-modified RCs of *Rb. sphaeroides* R-26 the appearance of the maximal emission at 935 nm is accompanied by the maximal bleaching at 800 nm and by the maximal formation of the 1020 nm band (*11, 12, 22*). This finding suggests that the wavepacket emitting light at the long-wavelength side of the stimulated emission band is located close to the intersection between the P^*B_A and $P^+B_A^-$ potential surfaces. Two vibrational modes at 30−33 and 130−140 cm^{-1} were found to have an intersection with the $P^+B_A^-$ surface (*11, 12*). Very recently a coherent component in the dynamics of population of the $P^+H_A^-$ state at 15 K has been demonstrated by observation of 30 cm^{-1} oscillations in the kinetics of the electrochromic shift of the absorption band at 800 nm in response to the electric field of the charge-transfer pair $P^+H_A^-$ (*10*).

Here we present the results showing that in *Rb. sphaeroides* R-26 RCs the wavepacket moving on the P* potential energy surface with a frequency of 130−140 cm^{-1} is transferred to the 32 cm^{-1} mode which belongs to the P* hypersurface or to the $P^+B_A^-$/P* diabatic surface. Finally an electron is accepted by H_A when the wavepacket is on the surface with $P^+B_A^-$ character. This conclusion was made on the basis of femtosecond measurements of the transient absorption spectra at different time delays in spectral regions covering P* stimulated emission (900−980 nm), B_A^- band formation (1000−1060 nm), and H_A band bleaching (720−780 nm) due to H_A^- formation.

MATERIALS AND METHODS

RCs of *Rhodobacter sphaeroides* R-26 were isolated as described in (*25*) and were pheophytin-modified as described in (*26*). The optical density of the samples was 0.5 at 860 nm at 293 K; 5 mM sodium dithionite was added to keep the state $PB_AH_AQ_A^-$ in RCs. All measurements were carried out at room temperature.

Femtosecond transient absorption measurements were carried out with a home-built amplified Ti:sapphire laser system with continuum generation and optical multichannel analyzer detection, described in detail in (*11*). The operating frequency was 15 Hz. The duration of pump and probe pulses was about 25 fs. Pump pulses were centered at 870 nm. The pump and probe pulses had weak (~20%) mutual perpendicular polarization while the remaining part (~80%) was depolarized. The delay between pump and probe pulses was changed with an accuracy of ~10 fs. The compression of

temporal dispersion in the range from 600 to 900 nm was monitored by kinetic measurements at 600 nm (Q_x transition of P) and at 900 nm (Q_y transition of P and the short-wavelength side of stimulated emission from P*). It was found to be less than 50 fs. Out-of-phase oscillation at 900 and 935 nm, observed earlier in (*17*−*20*), has shown that in this region the temporal dispersion was compressed to less than 10 fs. In-phase oscillation of the 935 and 1020 nm bands shown earlier (*11*, *12*) is consistent with the compression to less than 30 fs in the 930−1040 nm region. In agreement with this, it was found that the green filter (ZC-10) spectral band in the range of 935−1060 nm is bleached within 30 fs without any changes in the shape of this band.

The amplitudes of the spectral bands at 935, 1020, and 760 nm at different delays superimposed on the broad background were measured at their maxima as shown by the arrows in Figure 1. The resulting difference light-minus-dark time-resolved absorbance spectra were obtained by averaging 3000−7000 measurements at each delay. The accuracy of spectral measurements was (1−2) × 10^{-4} unit of optical density. The kinetics of absorbance changes (ΔA) of the mentioned bands were revealed from the difference absorbance spectra measured at different delays. The non-oscillating fits were subtracted from the kinetics, and the residual oscillatory parts of the kinetics were Fourier-transformed to obtain the spectra of oscillations. Note that the fits correspond to the minimal amplitude of the oscillations.

RESULTS

As mentioned, the excitation of P by ultrashort (<30 fs) pulses leads to the formation of the wavepacket and its motion on the P* hypersurface (with 130 cm^{-1} and other frequencies) accompanied by stimulated emission from P* with a time-dependent spectral position. It was shown that the oscillations in the stimulated emission are a result of the wavepacket motion within one electronic state (*17*−*21*). As shown below, spectral analysis of the formation of the 1020 nm band indicates that the femtosecond oscillations are related instead to the oscillations between different electronic states. The same conclusion can be found for the bleaching of the 760 nm band. Figure 1 depicts the spectra of absorbance changes in the ranges from 1000 to 1050 nm (development of the 1020 nm band of B_A^-), from 720 to 780 nm (H_A band bleaching due to H_A^- formation), and from 935 to 1050 nm (stimulated emission from P*, including 1020 nm band formation) at different delays in native RCs. The analysis of the data for 1020 nm band development ($P^+B_A^-$ formation) shows that the structure of this band (center position and shape) is not changed at different delays. This indicates that there are no any oscillations within one electronic state, $P^+B_A^-$. The appearance and subsequent disappearance of the 1020 nm band are instead related to the oscillations between the two states P* and $P^+B_A^-$ (see Discussion).

The spectrum of H_A^- formation was first characterized in nonpolarized light at room and at low temperature (*6*). Bleaching of the 760 nm band (Q_y transition of H_A), development of the broad 660 nm band (radical anion band of H_A^-), and the blue shift of the 800 nm band of B (development at 790 nm), with an amplitude ratio of 1:1.2:

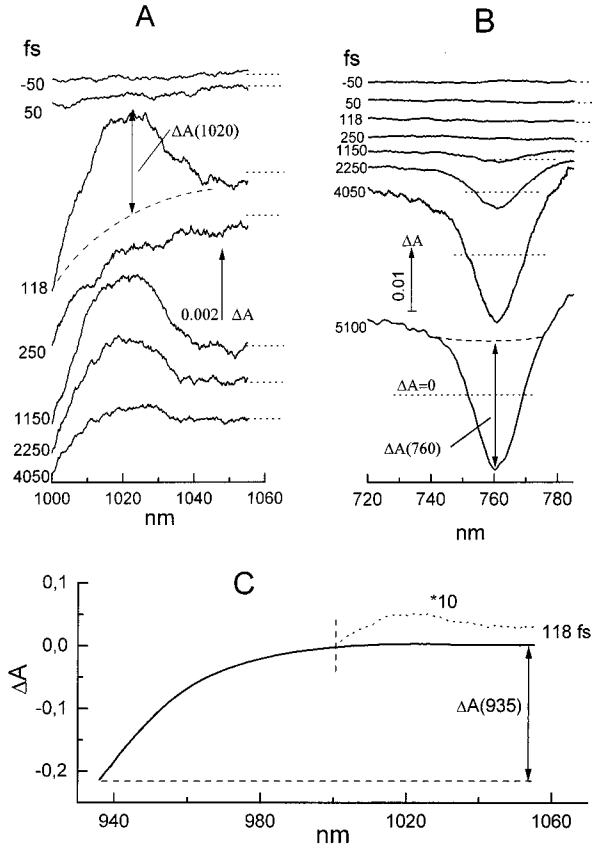

FIGURE 1: Difference (light-minus-dark) absorbance spectra measured at different femtosecond delays at 293 K in native *Rhodobacter sphaeroides* R-26 RCs excited by ~25 fs pulses at 870 nm. (A) Development of 1020 nm band of B_A^- at different delays. (B) Bleaching of H_A band at 760 nm at different delays. (C) Long-wavelength part of the stimulated emission from P* in the 935−1060 nm range at 118 fs delay; the kinetics in the range 1000−1050 nm are increased by a factor of 10 and normalized at 1000 nm with the nonincreased curve. Dotted lines show baselines for measured spectra. On the basis of measured spectra, the amplitudes of the corresponding ΔA indicated by arrows for 1020 nm band development (A), for 760 nm band bleaching (B), and for 935 nm stimulated emission (C) were determined.

1.4, respectively, were observed. Picosecond measurements in polarized light gave some different ratios of the mentioned amplitudes depending on the polarization of the transitions and the temperature of the sample. The ratio of $\Delta A(760)/\Delta A(787)$ was found to be 1:1.4 for the perpendicular polarization at 5 K (*27*). The spectrum at 5.1 ps presented in Figure 1B shows an $\Delta A(760)/\Delta A(780)$ ratio of 1:1.4, in agreement with (*6*).

The spectrum of the 760 nm band at different delays also shows that this band disappeared as a whole without any change in the central position and shape. The kinetics of the 760 nm band (see Figure 4A) demonstrate that this band irreversibly disappeared as an indicator of the irreversible electron transfer to H_A. These kinetics behave as an integral over the time of the kinetic peaks of the 1020 nm band, showing electron transfer from B_A^- to H_A (see below).

In previous experiments with Pheo-modified RCs of *Rb. sphaeroides* R-26, we have shown (*11*, *12*) that femtosecond kinetics of absorbance changes (ΔA) for the bands at 900 and 935 nm (P* stimulated emission) and 1020 nm (B_A^- band development), revealed from the difference absorption spectra taken at different femtosecond delays, allow visual-

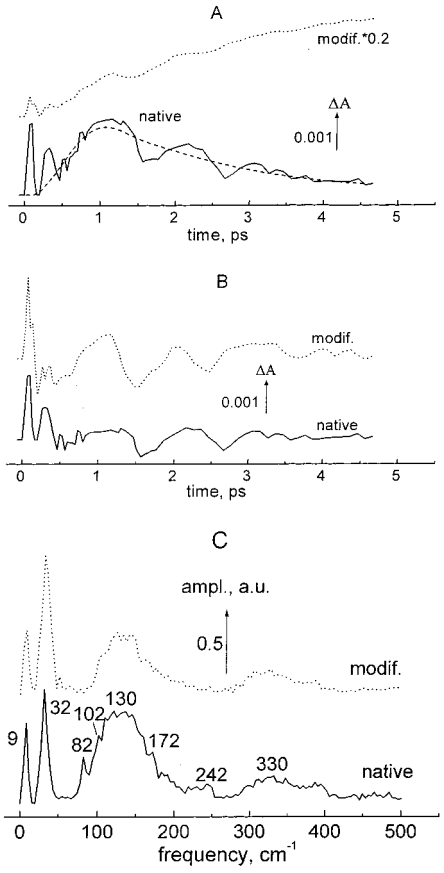

FIGURE 2: (A) Femtosecond kinetics of Δ*A* for 1020 nm band (B_A^-) development (see Figure 1A) for native (solid line) and pheophytin-modified (dotted line) RCs at 293 K. The dashed line represents a non-oscillating fit of the kinetics for native RCs. (B) Oscillatory parts of 1020 nm band kinetics for native (solid) and modified (dotted) RCs. (C) Fourier transform of the oscillatory parts of 1020 nm kinetics for native (solid) and modified (dotted) RCs.

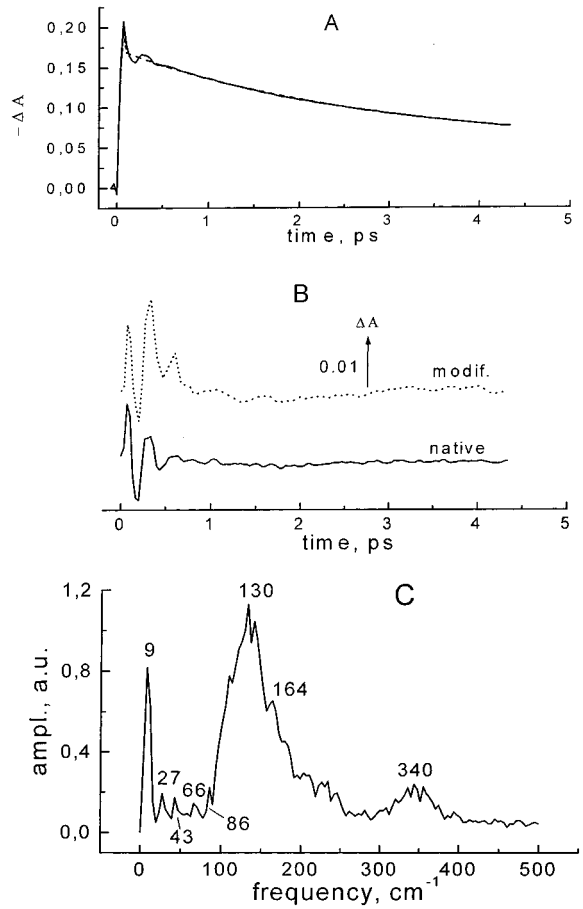

FIGURE 3: (A) Femtosecond kinetics of Δ*A* for the 935 nm band of the stimulated emission of P* (see Figure 1C) for native (solid line) RCs at 293 K. The dashed line represents a non-oscillating fit of the kinetics. (B) Oscillatory parts of the 935 nm band kinetics for native (solid) and modified (dotted) RCs. (C) Fourier transform of the oscillatory parts of the 935 nm kinetics for native RCs.

ization of the coupling of nuclear motions to ET from P* to B_A, resulting in the formation of the primary charge-transfer state $P^+B_A^-$. The development of the B_A^- absorption band at 1020 nm (measured on the broad background which arose due to the stimulated emission from P*; see, for example, Figure 1A,C for native RCs) was found to occur within ∼3 ps at room temperature (Figure 2A, dotted line). The accumulation of state $P^+B_A^-$ (no electron transfer from B_A^- to further acceptor takes place in Pheo-pheophytin RCs in this time domain) is accompanied by femtosecond oscillations which include two main vibrational modes with frequencies at 130−140 and 31−33 cm^{-1} (see Figure 2C, dotted line). The oscillations with a frequency at 130−140 cm^{-1} for 1020 nm band development are in-phase with those for the stimulated emission from P* at 935 nm (see Figures 2B and 3B, dotted lines).

Very similar room temperature oscillations in the femtosecond kinetics of 1020 nm absorption band development are demonstrated in Figure 2A−C (solid lines) for native RCs of *Rb. sphaeroides* R-26. Again, the kinetics were obtained from difference absorption spectra measured at different time delays (Figure 1A). The spectra and kinetics show that the B_A^- band at 1020 nm first appears at a delay of ∼120 fs with the amplitude comparable to that observed in Pheo-modified RCs (Figure 2B), and almost completely disappears at 250 fs. This reversible development of the 1020 nm absorption band is in-phase with the first appearance of the emission peak on the long-wavelength side of the stimulated emission band at 935 nm (Figures 2 and 3), in agreement with measurements performed on the Pheo-modified RCs [dotted lines and (*11*, *12*)]. The second appearance of the 1020 nm band observed at ∼380 fs (the ∼260 fs period of these oscillations corresponds to a frequency of ∼130 cm^{-1}) is in-phase with the stimulated emission at 935 nm and is about 70% reversible (Figure 2A). Next, three features reflecting oscillations of the 1020 nm band are clearly seen at ∼1.15 ps (∼50% reversibility), ∼2.17 ps, and 3.14 ps with a half-width of about 680 fs are observed (∼1 ps period corresponds to a frequency of ∼33 cm^{-1}). In contrast to Pheo-modified RCs (Figure 2A, dotted line), in native RCs the non-oscillating amplitude of the 1020 nm band (dashed line in Figure 2A) was estimated to increase within ∼0.9 ps and to decrease within ∼2.5 ps due to electron transfer from P* to B_A (∼2.5 ps) and from B_A^- to H_A (∼0.9 ps), in agreement with previous estimations (*2*).

Figure 2C depicts the results of FT for the oscillatory part of the 1020 nm band kinetics shown in Figure 2B. The FT spectra for Pheo-modified and native RCs are very similar to each other. In agreement with a preliminary assignment, two main bands for both Pheo-modified and native RCs are observed at 32 cm^{-1} (narrow) and 130 cm^{-1} (broad). The frequency components at about 9, 82, 102, 172, 242, and

330 cm^{-1} (broad) are also seen in the FT spectra for native RCs.

Figure 3 shows the kinetics at 935 nm (the long-wavelength side of the P* stimulated emission band) (A), the oscillatory part of these kinetics (B), and FT of the oscillatory part (C). As mentioned, the peaks in the oscillatory feature of the stimulated emission at 120 and 380 fs coincide with the corresponding peaks in the 1020 nm band kinetics for Pheo-modified and native RCs (Figures 2 and 3). This observation suggests that the product ($P^+B_A^-$) appears when the wavepacket approaches the long-wavelength side of the emission band. Thus, the intersection of the potential energy surfaces of P* (130−140 cm^{-1} mode) and $P^+B_A^-$ seems to occur at this side.

The FT spectrum for the 935 nm kinetics (Figure 3C) includes several bands at about 9, 27, 43, 66, 86, 130 (br), 164, and 340 cm^{-1} (br). The bands at 9 and 130 cm^{-1} have maximal amplitude. This spectrum is very similar to that observed previously for the 890 nm kinetics in native RCs (bands at 9, 27, 42, 84, and 124 cm^{-1} were registered) (*22*). Notably, the 27 cm^{-1} mode seen in both spectra for the 935 and 890 nm kinetics has no counterpart in the FT spectrum for the 1020 nm kinetics. The 32 cm^{-1} mode found for the 1020 nm kinetics differs from the 27 cm^{-1} mode both in amplitude and in frequency position. The modes with frequencies at 130−140 and 330−340 cm^{-1} are similar for the kinetics of the 1020 and 935 nm bands.

The characteristic feature of the 130−140 cm^{-1} vibrational mode is its high *S*-factor value (∼2) found from hole burning experiments (*13*) and from simulation of the P absorbance spectra of RCs (*23, 24*). It was concluded that the 130−140 cm^{-1} vibrational levels are directly populated by light excitation at 870 nm since the relatively weak 0−0 transition of P is located near 907 nm (*23*). Therefore, the excitation of P near 870 nm is accompanied by the population of 2d or 3d levels of the 130−140 cm^{-1} mode, in agreement with FT spectra of femtosecond kinetics. On the other hand, a relatively small *S*-factor was found for the 27 cm^{-1} mode which was assigned to a protein phonon wing (*13*). The population of the 32 cm^{-1} mode is probably absent when P is directly excited.

Figure 4A (solid line) demonstrates the kinetics of bleaching of the Q_y absorption band of the photochemically active bacteriopheophytin (H_A) at 760 nm due to the formation of state $P^+H_A^-$ in native RCs of *Rb. sphaeroides* R-26 at room temperature. The amplitude of 760 nm band bleaching (ΔA_{760}) was calculated from the difference absorption spectra presented in Figure 1B. The oscillatory part is depicted in Figure 4B and its FT in Figure 4C. No electron transfer to H_A is observed when B_A^- appears at 120 fs and a little at 380 fs delay. One can assume that the 32 cm^{-1} mode includes the appearance of the wavepacket on the $P^+B_A^-$ surface at ∼1.15, ∼2.17, and ∼3.14 ps delays accompanied by electron transfer to H_A. An analysis of the kinetics of the 1020 and 760 nm bands shows that a rise of the bleaching of the 760 nm band represents roughly the integration over time of the 1020 nm oscillatory peaks at ∼1.15, ∼2.17, and ∼3.14 ps superimposed on the exponential growth. It means that the motion of the wavepacket on the surface with $P^+B_A^-$ character is accompanied by electron transfer to H_A. The measurements at 90 K (Figure 4A, dotted line) indicate that such an integration is observed at much earlier time when

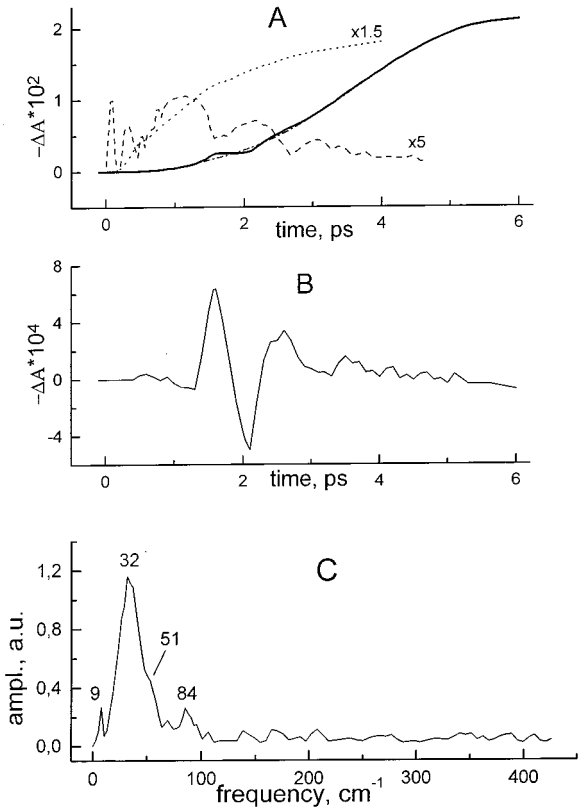

FIGURE 4: (A) Femtosecond kinetics of ΔA for 760 nm band (H_A) bleaching (see Figure 1B) for native (solid line) RCs at 293 K. The dashed−dotted line represents a non-oscillating fit of the kinetics for native RCs. The dashed line indicates the 1020 nm kinetics taken from Figure 2A. The dotted line depicts the 760 nm kinetics for native RCs at 90 K. (B) Oscillatory part of 760 nm band kinetics at room temperature. (C) Fourier transform of the oscillatory parts of the kinetics.

the 1020 nm peak appears at 380 fs (remaining data will be published in future work).

It should be noted that the one-wavelength kinetic measurements with respect to the zero line are not able to show real H_A band bleaching until at least a delay when "pure" bleaching below the zero line is detected. For example, in (*28*) these kinetic measurements with respect to the zero line were done at 760 nm, which included the formation and decay of P*, $P^+B_A^-$, and $P^+H_A^-$. However, even in this complicated case, the start of the absorbance decrease at 760 nm was registered beginning from the 1 ps delay and the "pure" bleaching (below the zero line) from 2 ps. This is consistent with the spectra and kinetics presented in Figures 1 and 4. In (*29*), the bleaching at 760 nm shown by the solid line in Figure 2 of (*29*) was started from 1 ps delay; however, the signal/noise ratio was not enough to measure this time region in detail. This was done in the present work and is demonstrated in Figures 1 and 4.

The FT spectrum of the oscillatory part of the 760 nm band kinetics (Figure 4C) shows that the spectrum includes one main band at 32 cm^{-1}, in agreement with the measurements at 788 nm at low temperature (*10*). Since this frequency is the same as for 1020 nm band kinetics, this finding supports the idea that the 32 cm^{-1} mode reflects the motion of the wavepacket between states P* and $P^+B_A^-$ accompanied by electron transfer to H_A.

The FT spectrum for 760 nm band kinetics also includes small bands at 9, 51 (sh), and 84 cm^{-1}. The origin of the 9

cm^{-1} band seen in all spectra is not completely clear. Simulations show that it can be related to some distortion during a procedure of the FT. The bands near 84 cm^{-1} are observed in the 1020 nm (82 cm^{-1}) and the 935 nm (86 cm^{-1}) FT spectra.

One can compare our results with those published by Vos et al. (*10*) for $P^+H_A^-$ formation measured at 788 nm at 15 K. Despite the presence of a lag in H_A reduction at 293K (Figure 4) which is absent at 15 K (*10*), the oscillatory parts of both kinetics are very similar to each other. The FT spectra of these kinetics presented in Figure 3 of (*10*) and in our Figure 4 are identical as well and show remarkable contribution of the 30−32 cm^{-1} mode in the oscillations. The whole kinetics at 760 nm measured at 90 K (Figure 4A) are very similar to those measured at 788 nm at 15 K by Vos et al. (*10*). Results published in (*30*) for 800 nm band oscillations demonstrated a remarkable contribution of the 32 cm^{-1} mode as well. From comparison of the data, it is clear that the lag in the reduction of H_A is temperature-dependent and has important physical meaning (to be published in the future).

DISCUSSION

The picosecond, femtosecond, and Raman studies of the primary charge separation and vibronic structure of photoactive chromophores in bacterial RCs are widely described in the literature (*1*−*8, 14*−*16, 23, 24, 26*−*29, 31*−*39*). A new tool for detecting low-frequency nuclear motion in RCs based on femtosecond spectroscopy is developed in (*10*−*12, 17*−*22, 40*−*42).* Here this tool was applied to the study of electron−nuclear coupling during the charge separation process in RCs.

Various theoretical models, for example, the Marcus model (*43*) and vibration overlap models (*44*), studied the charge separation process and electron-transfer reactions in RCs. Quantum chemical methods were used to find wave functions, energies, and coupling parameters (*45*−*50*). The above-described results allow one to draw the potential energy scheme for nonequilibrium conversion of the excited-state P* into the charge-separated states $P^+B_A^-H_A$ and $P^+B_AH_A^-$ in bacterial reaction centers. The first step of the conversion was theoretically described in (*48*) by a harmonic bath model with the electronically diabatic (phonon) Hamiltonians for the ground (PB_A, H_1), locally excited (P^*B_A, H_2), and charge-transfer ($P^+B_A^-$, H_3) states. The reaction coordinates Q_1 and Q_2 (*48*) are defined for the photoexcitation and the electron-transfer processes, respectively. The angle (θ) between Q_1 ($\equiv\Sigma_i\xi_i x_i$) and Q_2 ($\equiv\Sigma_i\xi_i' x_i + \Sigma_j\eta_j y_j$) determines the amplitude of femtosecond oscillation of the electron-transfer rate treated by the Landau−Zener semiclassical approach: when $\cos\theta = -1$ (linear arrangement), the oscillations are maximal; when $\cos\theta = 0$ (orthogonal arrangement), the oscillations are absent. The same is true for the average femtosecond motion of the *x*-part of the reaction coordinate (*48*):

$$Q_{2x}(t) = \Sigma_i\xi_i\xi_i' \cos(\omega_i t)/(\hbar\omega_i) \qquad (1)$$

Oscillations of $Q_{2x}(t)$ are maximal when $\cos\theta = -1$, and minimal in the orthogonal case ($\cos\theta = 0$). The remarkable oscillations in the product $P^+B_A^-$ at 1020 nm indicate that the angle θ is close to 180° (and $\cos\theta \approx -1$). Therefore, one can cut the diabatic potential energy surfaces along the Q_1 and Q_2 coordinates. The results of a one-dimension cross section are shown in Figure 5.

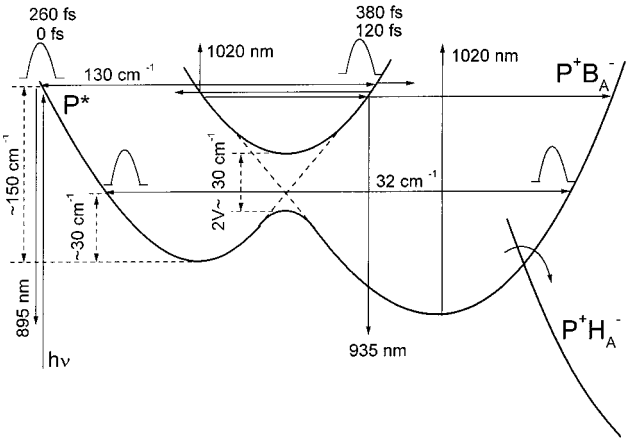

FIGURE 5: Schematic representation of the diabatic (phonon) potential energy surfaces of the locally excited ($P^*B_AH_A$), and charge-transfer ($P^+B_A^-H_A$ and $P^+B_AH_A^-$) states. An electronic coupling between P* and B_A (*50*) splits two original surfaces (P* and $P^+B_A^-H_A$) into two upper and lower parts. The 130 cm^{-1} wavepacket can approach the upper part of the $P^*B_AH_A/P^+B_A^-H_A$ surface and produce emission at 935 nm (P*) and absorption at 1020 nm (B_A^-) indicated by arrows. The 32 cm^{-1} vibrational mode represents the wavepacket motion on the P* hypersurface or on the mixing diabatic surface (lower part) including the P* and $P^+B_A^-H_A$ states. The wavepacket on the $P^+B_A^-H_A$ part of such a surface has absorption at 1020 nm (B_A^-) indicated by the arrow. The $P^+B_AH_A^-$ surface is suggested to cross the mixing surface at its part having charge-transfer character ($P^+B_A^-H_A$). According to Figure 4, the transmission coefficient at the corresponding crossing can be quite large and approach the adiabatic limit.

The transmission coefficient *k* at the crossing of the P* and $P^+B_A^-$ surfaces can be written as follows (*48*):

$$k(\dot{Q}) \equiv P_{LZ}(|\dot{Q}|)\theta(\dot{Q}) + P_{LZ}(|\dot{Q}|)/[1 + P_{LZ}(|\dot{Q}|)] \qquad (2)$$

where $\theta(x)$ is the Heaviside unit function and $P_{LZ}(|\dot{Q}|)$ is the transition probability per crossing, for which the following Landau−Zener form is assumed:

$$P_{LZ}(|\dot{Q}|) = 1 - \exp[-2\pi J^2/(\hbar|\dot{Q}|)] \qquad (3)$$

where *J* is the electronic coupling for the ET.

The results show that in RCs the wavepacket is initially formed by femtosecond light pulses on the 130−140 cm^{-1} potential energy surface of P* at the short-wavelength side of the stimulated emission band from P* (895 nm). No $P^+B_A^-$ is observed at this side. Subsequent motion of the wavepacket on the 130−140 cm^{-1} surface toward the long-wavelength side (935 nm) of the stimulated emission band leads it to the intersection region between P* and $P^+B_A^-$ surfaces at 120 fs delay.

The estimation of the wavepacket energy above the bottom of the P* surface gives a value of about 150 cm^{-1} [11 173 cm^{-1} (895 nm) − 11 025 cm^{-1} (907 nm as 0−0 transition)]. The intersection point is above the bottom by ~30 cm^{-1} (*12*). Therefore, the first at 120 fs and second at 380 fs approaches of the wavepacket to the intersection region should be above the intersection point by ~120 cm^{-1}. According to (*48*), in this region reflections from walls of both wells (for P* and $P^+B_A^-$ surfaces) are possible. The wavepacket at the P* surface wall emits light at 935 nm, and that at the $P^+B_A^-$ surface wall absorbs light at 1020 nm. Figures 2 and 3 show

that relative amplitudes of the oscillations at 120 fs delay for the 935 and 1020 nm bands are very similar in pheophytin-modified RCs [see also (*12*)] as measured with respect to the maximal amplitudes of the corresponding ΔA found at 5 ps (0.19:0.20, respectively). This fact might suggest that each wavepacket approaching the long-wavelength side of the stimulated emission at 935 nm approaches the $P^+B_A^-$ surface as well. However, no wavepacket transfer from the P* to $P^+B_A^-$ surface and no electron transfer to H_A are observed at 120 fs since the 1020 nm band disappears at longer (250 fs) delay and no remarkable bleaching of the 760 nm band is observed at this delay. It means that all wavepackets at 120 fs (and most of them at 380 fs) are reflected back to the left side of the P* surface. [The picture seems to be different at low temperature when the transmission through the P* surface wall becomes much greater at 380 fs delay (see Figure 4A and second part of this work to be published in the future).] Only after several reflections and loss of some energy does the wavepacket approach the intersection region close to the intersection point at $\sim$30 cm^{-1} above the bottom. At this point, the electronic coupling for ET (*50*) splits two surfaces into two new wells (see Figure 5).

Let us start a discussion of two possible explanations of the wavepacket motion on the 32 cm^{-1} surface.

I. Final electron transfer to H_A can be good evidence for wavepacket appearance on the surface with $P^+B_A^-$ character according to the sequential model of ET. The main frequency component for $P^+H_A^-$ formation measured at 760 nm is located at 32 cm^{-1} [see Figure 4C and (*10*)]. It means that this frequency can be related to the appearance of the wavepacket on the surface with $P^+B_A^-$ character, which makes possible the electron transfer to H_A. In fact, the same frequency (32 cm^{-1}) is also the main frequency for $P^+B_A^-$ formation measured at 1020 nm (Figure 2C). These results indicate two important points: (i) the wavepacket is transferred to the surface with $P^+B_A^-$ character during motion with a frequency of 32 cm^{-1}; (ii) the appearance of the wavepacket on the surface with $P^+B_A^-$ character leads to a very effective electron transfer to H_A revealed by the same frequency in agreement with the sequential model of ET.

The 32 cm^{-1} mode was observed earlier for $P^+B_A^-$ accumulation in Pheo-modified and native RCs (*11, 12, 22, 30*). It was suggested that this mode is related to the oscillation on the P* surface. However, the 27 cm^{-1} mode observed in hole-burning (*13*) and for femtosecond kinetics of the stimulated emission at 890 nm (*22*) and 935 nm (Figure 3) is different from the 32 cm^{-1} mode in frequency position and shows a peak of relatively small amplitude in the FT spectra. On the other hand, the frequencies in the FT spectrum for the 935 nm kinetics (Figure 3C) at 66, 100 (sh), 130, and 164 cm^{-1} might be interpreted as overtone frequencies (calculated as 64, 96, 128, and 160 cm^{-1}) for a fundamental one at 32 cm^{-1}. (The physical basis for the appearance of higher harmonics of the 32 cm^{-1} mode will be discussed in the second part of this work to be published elsewhere.) Earlier similar frequencies have been found in femtosecond kinetic measurements at low temperature (*19*). These results can show that the formation of the wavepacket with a frequency of 130−140 cm^{-1} on the hypersurface of P* leads to the subsequent population of the 32 cm^{-1} mode and its overtones. This can be possible since the wavepacket energy for the 130−140 cm^{-1} mode is about 5 times larger than that for the 32 cm^{-1} mode. If it is true, the 32 cm^{-1} mode might belong to the P* hypersurface as well. Then the appearance of the wavepacket on the $P^+B_A^-$ surface with a frequency of 32 cm^{-1} is a result of wavepacket motion on the P* surface with the same frequency and effective transmission of the wavepacket to the $P^+B_A^-$ surface and then from that to the $P^+H_A^-$ surface.

II. The alternative consideration of the nature of the 32 cm^{-1} mode observed for both Pheo-modified and native RCs can give another picture. The probability of wavepacket transfer directly from the intersection point between the P* and $P^+B_A^-$ surfaces to the $P^+H_A^-$ surface is too small since there is probably no intersection of three surfaces at the same point. This is supported by the fact that the kinetics for the 1020 and 760 nm bands are different and show some delay of 760 nm band bleaching with respect to 1020 nm band development (Figures 2 and 4). Simulation of the process shows that the kinetics of 760 nm band bleaching reflect the integration of the 1020 nm peaks over time. Therefore, we can assume that the 32 cm^{-1} mode includes motions on both the P* and $P^+B_A^-$ surfaces along coordinate Q_2 which allow the electron transfer to H_A when the wavepacket is on the $P^+B_A^-$ part of the 32 cm^{-1} surface (Figure 5). In other words, the P* and $P^+B_A^-$ states can form a diabatic surface, part of which has $P^+B_A^-$ charge-transfer character. Wavepacket motion between P* and $P^+B_A^-$ might have sufficient probability if this motion includes the distance and orientation changes between P and B_A shown by molecular dynamics calculations for two modes at 17 and 28 cm^{-1} (*49*).

The kinetics for the 1020 nm band have very similar oscillatory parts for both native and Pheo-modified RCs (Figure 2B). In the latter case, the 32 cm^{-1} oscillation observed for 1020 nm band kinetics can correspond only to the oscillation of the wavepacket between two surfaces of P* and $P^+B_A^-$ (no electron transfer to H_A is observed in the picosecond time domain in modified RCs). In native RCs, the appearance of the main peaks in the 760 nm band kinetics coincides with the ends of the 1020 nm band peaks (Figures 2 and 4). As indicated above, the simulation of the process shows that the kinetics of 760 nm band bleaching reflect the integration of the 1020 nm peaks over time. It is reasonable since the appearance of the wavepacket on the $P^+B_A^-$ part of the surface leads to electron transfer to H_A proportionally to the time the wavepacket is on the $P^+B_A^-$ part of the surface.

ACKNOWLEDGMENT

We thank Dr. A. V. Sharkov for help in maintenance of the femtosecond spectrometer and V. A. Shkuropatova for preparing the samples.

REFERENCES

1. Woodbury, N. W., Becker, M., Middendorf, D., and Parson, W. W. (1985) *Biochemistry 24*, 7516−7521.
2. Schmidt, S., Arlt, T., Hamm, P., Huber, H., Nagele, T., Wachtveitl, J., Meyer, M., and Scheer H. (1995) *Spectrochim. Acta, Part A 51*, 1565−1578.
3. Kennis, J. T. M., Shkuropatov, A. Ya., Van Stokkum, I. H. M., Gast, P., Hoff, A. J., Shuvalov, V. A., and Aartsma, T. J. (1997) *Biochemistry 36*, 16231−16238.
4. Lauterwasser, C., Finkele, U., Scheer, H., and Zinth, W. (1991) *Chem. Phys. Lett. 183*, 471−477.

5. Fleming, G. R., Martin, J.-L., and Breton, J. (1988) *Nature 333*, 190−192.
6. Shuvalov, V. A., and Klimov, V. V. (1976) *Biochim. Biophys. Acta 440*, 587−599.
7. Shuvalov, V. A., and Yakovlev, A. G. (1998) *Membr. Cell Biol. 12*, 563−569.
8. Nowak, F. R., Kennis, J. T. M., Franken, E. M., Shkuropatov, A. Ya., Yakovlev, A. G., Gast, P., Hoff, A. J., Aartsma, T. J., and Shuvalov, V. A. (1998) *Proceedings of the XIth International Congress on Photosynthesis*, pp 783−786, Budapest, Hungary, Kluwer Academic Publishers, Dordrecht, The Netherlands.
9. Bixon, M., Jortner, J., Plato, M., and Michel-Beyerle, M. E. (1988) in *The Photosynthetic Bacterial Reaction Center. Structure and Dynamics* (Breton, J., and Vermeglio, A., Eds.) pp 399−419, Plenum Press, New York and London.
10. Vos, M. H., Rischel, C., Jones, M. R., and Martin, J.-L. (2000) *Biochemistry 39*, 8353−8361.
11. Yakovlev, A. G., Shkuropatov, A. Ya., and Shuvalov, V. A. (2000) *FEBS Lett. 466*, 209−212.
12. Yakovlev, A. G., and Shuvalov, V. A. (2000) *J. Chin. Chem. Phys. 47*, 709−714.
13. Shuvalov, V. A., Klevanik, A. V., Ganago, A. O., Shkuropatov, A. Ya., and Gubanov, V. S. (1988) *FEBS Lett. 237*, 57−60.
14. Shreve, A. P., Cherepy, N. J., Franzen, S., Boxer, S. G., and Mathies, R. A. (1991) *Proc. Natl. Acad. Sci. U.S.A. 88*, 11207−11211.
15. Cherepy, N. J., Shreve, A. P., Moore, L. J., Franzen, S., Boxer, S. G., and Mathies, R. A. (1994) *J. Phys. Chem. 98*, 6023−6029.
16. Palaniappan, V., Aldema, M. A., Frank, H. A., and Bocian, D. F. (1992) *Biochemistry 31*, 11050−11058.
17. Vos, M. H., Rappaport, F., Lambry, J.-C., Breton, J., and Martin, J.-L. (1993) *Nature 363*, 320−325.
18. Vos, M. H., Jones, M. R., McGlynn, P., Hunter, C. N., Breton, J., and Martin, J.-L. (1994) *Biochim. Biophys. Acta 1186*, 117−122.
19. Vos, M. H., Jones, M. R., Hunter, C. N., Breton, J., Lambry, J.-C., and Martin, J.-L. (1994) *Biochemistry 33*, 6750−6757.
20. Vos, M. H., Jones, M. R., Hunter, C. N., Breton, J., and Martin, J.-L. (1994) *Proc. Natl. Acad. Sci. U.S.A. 91*, 12701−12705.
21. Spörlein, S., Zinth, W., and Wachtveitl, J. (1998) *J. Phys. Chem. B 101*, 7492−7496.
22. Streltsov, A. M., Vulto, S. I. E., Shkuropatov, A. Ya., Hoff, A. J., Aartsma, T. J., and Shuvalov, V. A. (1998) *J. Phys. Chem. B 102*, 7293−7298.
23. Klevanik, A. V., Ganago, A. O., Shkuropatov, A. Ya., and Shuvalov, V. A. (1988) *FEBS Lett. 237*, 61−64.
24. Lyle, P. A., Kolaczkowsky, S. V., and Small, G. J. (1993) *J. Phys. Chem. 97*, 6924−6933.
25. Shuvalov, V. A., Shkuropatov, A. Y., Kulakova, S. M., Ismailov, M. A., and Shkuropatova, V. A. (1986) *Biochim. Biophys. Acta 849*, 337−348.
26. Shkuropatov, A. Y., and Shuvalov, V. A. (1993) *FEBS Lett. 322*, 168−171.
27. Kirmair, C., Holten, D., and Parson, W. (1985) *Biochim. Biophys. Acta 810*, 49−61.
28. Chekalin, S. V., Matveetz, Yu. A., and Shkuropatov, A. Ya. (1987) *FEBS Lett. 216*, 245−248.
29. Streltsov, A. M., Yakovlev, A. G., Shkuropatov, A. Ya., and Shuvalov, V. A. (1996) *FEBS Lett. 383*, 129−132.
30. Streltsov, A. M., Aartsma, T. J., Hoff, A. J., and Shuvalov, V. A. (1997) *Chem. Phys. Lett. 266*, 347−352.
31. Arlt, T., Schmidt, S., Kaiser, W., Lauterwasser, C., Meyer, M., Scheer, H., and Zinth, W. (1993) *Proc. Natl. Acad. Sci. U.S.A. 90*, 11757−11761.
32. Schmidt, S., Arlt, T., Hamm, P., Huber, H., Nagele, T., Wachtveitl, J., Meyer, M., Scheer, H., and Zinth, W. (1994) *Chem. Phys. Lett. 223*, 116−120.
33. Zinth, W., Huppmann, P., Arlt, T., and Wachtveitl, J. (1998) *Philos. Trans. R. Soc. London, Ser. A 356*, 465.
34. Huber, H., Meyer, M., Scheer, H., Zinth, W., and Wachtveitl, J. (1998) *Photosynth. Res. 55*, 153−168.
35. Vos, M. H., Lambry, J.-C., St. Robles, J., Youvan, D. C., Breton, J., and Martin, J.-L. (1991) *Proc. Natl. Acad. Sci. U.S.A. 88*, 8885−8889.
36. Cherepy, N. J., Holtzwarth, A. R., and Mathies, R. A. (1995) *Biochemistry 34*, 5288−5293.
37. Cherepy, N. J., Shreve, A. P., Moore, L. J., Boxer, S. G., and Mathies, R. A. (1997) *Biochemistry 36*, 8559−8566.
38. Cherepy, N. J., Shreve, A. P., Moore, L. J., Boxer, S. G., and Mathies, R. A. (1997) *J. Phys. B 101*, 3250−3260.
39. Palaniappan, V., Schenk, C. C., and Bocian, D. F. (1995) *J. Phys. Chem. 99*, 17049−17058.
40. Vos., M. H., Jones, M. R., Breton, J., Lambry, J.-C., and Martin, J.-L. (1996) *Biochemistry 35*, 2687−2692.
41. Vos, M. H., Jones, M. R., and Martin, J.-L. (1998) *Chem. Phys. 233*, 179−190.
42. Vos, M. H., Rischel, C. R., Breton, J., Martin, J.-L., Ridge, J. P., and Jones, M. R. (1998) *Photosynth. Res. 55*, 181−187.
43. Marcus, R. A. (1964) *Annu. Rev. Phys. Chem. 15*, 155−196.
44. Jortner, J. (1980) *J. Am. Chem. Soc. 102*, 6676−6686.
45. Kitzing, E., and Kuhn, H. (1990) *J. Phys. Chem. 94*, 1699−1715.
46. Larsson, S., Broo, A., Kallebring, B., and Volosov, A. (1988) *Int. J. Quantum Chem., Quantum Biol. Symp. 15*, 1−22.
47. Larsson, S., and Ivashin, N. V. (1999) *J. Appl. Spectrosc. 66*, 539−543.
48. Ando, K., and Sumi, H. (1998) *J. Phys. Chem. B 102*, 10991−11000.
49. Parson, W. W., Chu, Z. T., and Warshel, A. (1998) *Photosynth. Res. 55*, 147−152.
50. Zhang, L. Y., and Friesner, R. A. (1998) *Proc. Natl. Acad. Sci. U.S.A. 95*, 13603−13605.

BI0101244